JACS
JOURNAL OF THE AMERICAN CHEMICAL SOCIETY
pubs.acs.org/JACS
Article

Efficient High-Order Harmonic Generation from the van der Waals Layered Crystal Copper Indium Thiophosphate

Aamir Mushtaq, Troie Journigan, Volodymyr Turkowski, Ryan Siebenaller, Dylan A. Jeff, Tran-Chau Truong, Mohamed Yaseen Noor, Dipendra Khatri, Christopher Lantigua, Kamal Harrison, Saiful I. Khondaker, Emmanuel Rowe, Jonathan T. Goldstein, Michael A. Susner, Enam Chowdhury, and Michael Chini*

Cite This: J. Am. Chem. Soc. 2024, 146, 24288−24295

Read Online

ACCESS | Metrics & More | Article Recommendations | Supporting Information

ABSTRACT: Layered metal thio- and selenophosphates (MTPs) are a family of van der Waals gapped materials that exhibit a multitude of functionalities in terms of magnetic, ferroelectric, and optical properties. Despite the recent progress in terms of understanding the material properties of these compounds, the potential of MTPs as a material class yet needs further scrutiny, especially in terms of nonlinear optical properties. Recent reports of efficient low-order harmonic generation and extremely high third-order nonlinear optical properties in MTPs suggest the potential application of these materials in integrated nanophotonics. In this article, we investigate the high-order nonlinear response of bulk and exfoliated thin-film crystals of copper indium thiophosphate (CIPS) to intense mid-infrared fields through experimental and computational studies of high-order harmonic generation (HHG). From a driving laser source with a 3.2 μm wavelength, we generate odd and even harmonics up to the 10th order, exceeding the bandgap of the material. We note conversion efficiencies as high as 10^{-7} measured for the fifth and seventh harmonics and observe that the harmonic intensities follow a power law scaling with the driving laser intensity, suggesting a perturbative nonlinear optical origin of the observed harmonics for both bulk and thin flakes. Furthermore, first-principles calculations suggest that the generation of the highest harmonic orders results from electron−electron interactions, suggesting a correlation-mediated enhancement of the high-order optical nonlinearity.

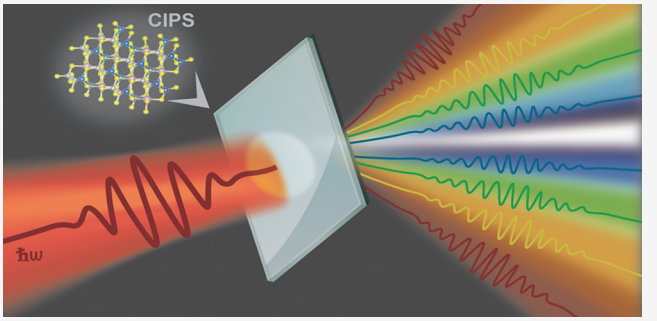

INTRODUCTION

The strong-field nonlinear response of a material under the influence of an intense, low-frequency femtosecond laser field is progressively being exploited for the high-order harmonic generation (HHG) of coherent high-frequency light. HHG harnesses the electron dynamics driven by intense, low-frequency driving lasers to produce high-energy photons which can be applied for time-resolved spectroscopy, metrology, or imaging applications.[1] As the emission of HHG from solids is a consequence of microscopic laser-driven currents, the same physics can be harnessed for the development of lightwave electronics devices operating at optical frequencies.[2,3]

HHG and other strong-field processes have been well studied in atomic and molecular gases.[4] More recently, long-wavelength driving laser fields in the mid-infrared spectral region have enabled the experimental observation of HHG from solid-state samples.[1,5,6] The advancement of high-order harmonic spectroscopy and the application of intense, low-frequency fields in novel optoelectronic devices necessitate the exploration of new nonlinear optical (NLO) materials with optical and chemical stability to generate coherent short-wavelength light sources and to convert long-wavelength laser light into petahertz-frequency electronic signals. Conventional nonlinear photonic devices which are based on bulk lithium niobate ($LiNbO_3$) and barium titanate ($BaTiO_3$) pose limitations such as low nonlinear susceptibility and phase matching issues which make them ill-suited for future nonlinear photonic devices.[6] While HHG in solids stems from a weaker polarization response than low-order nonlinearities, it is a near-universal phenomenon that can be realized in a wide array of material systems without phase matching, and therefore, it may be leveraged for novel nanophotonic devices if suitable materials with high conversion efficiency can be found.

Received: April 2, 2024
Revised: August 12, 2024
Accepted: August 13, 2024
Published: August 22, 2024

https://doi.org/10.1021/jacs.4c04515
J. Am. Chem. Soc. 2024, 146, 24288−24295

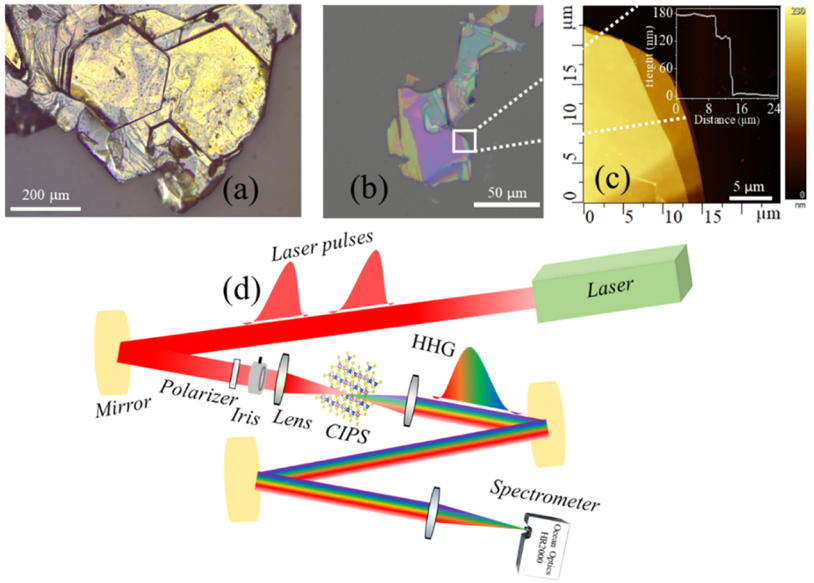

Figure 1. (a) Optical image of as-grown CIPS crystal. (b) Mechanically exfoliated CIPS flakes. (c) AFM image of the marked region with the inset showing the height profile of exfoliated CIPS obtained from the marked region. (d) Cartoon depicting experimental setup used for HHG in CIPS.

Recently, two-dimensional (2D) layered materials beyond graphene have emerged as ideal candidates for photonic devices based on their observed extraordinary nonlinear light–matter interactions,[7,8] thus enabling several fundamental discoveries in nonlinear optics.[6] Compared to graphene and transition metal dichalcogenides like MoS_2 and WSe_2, layered quaternary metal thio- and selenophosphates (MTPs) are newcomers to this field.[9] This class of exotic materials has a general compositional scheme of $A^{1+}M^{3+}[P_2X_6]^{4-}$ where A = Li, Cu, or Ag; M = Al, Sc, In, Cr, V, Bi, etc., and X is the chalcogenide element (S or Se). MTPs are made of vertically stacked layers which are held together via weak van der Waals interactions. MTPs are considered as structural analogues of metal dichalcogenides in which 1/3 of the metal atoms are substituted by a diphosphorous entity that covalently bind six adjacent chalcogen atoms into the anionic $[P_2X_6]^{4-}$ subgroup. This unit is then charge balanced against the positive charge carried by the metal cations, thus creating a unique mixture of ionic, covalent, and van der Waals bonding in these materials.[9] Among MTPs, copper indium thiophosphate, $CuInP_2S_6$ (CIPS), is one of the representative materials that has gained much recent interest due to its chemical stability, room-temperature ferroelectricity, and spontaneous polarization.[10] These properties have made CIPS an appealing candidate for MTP-based optoelectronics. Recent reports on CIPS and Cu-deficient CIPS suggested that CIPS possess outstanding third-order nonlinearity, as evidenced by strong two photon absorption (2PA) and nonlinear refractive index.[11,12] It has been inferred that the 2PA coefficient of CIPS is comparable to or higher than that of most conventional semiconductors and NLO crystals like $KTiOPO_4$.[11,12] Furthermore, there are multiple reports on extraordinary second-order nonlinear properties of CIPS. Lu et al. and co-workers observed that local strain-induced nanoengineering of CIPS results in an ∼160-fold increase in the efficiency of second harmonic generation (SHG) compared to an unstrained sample, which could make them ideal for flexible optoelectronics applications.[13] Analogously, silver indium thiophosphate ($AgInP_2S_6$) nanosheets exhibit layer-dependent SHG.[14] It is interesting to note that bulk crystalline $AgInP_2S_6$ has inversion symmetry, whereas $CuInP_2S_6$ bulk crystals are noncentrosymmetric. Therefore, one can expect the generation of even and odd harmonics in CIPS irrespective of the number of layers present.

Here, we demonstrate the efficient generation of high-order harmonics up to the 10th harmonic order from bulk and thin flakes of the van der Waal layered crystal CIPS using femtosecond mid-infrared laser pulses, without damaging the sample. Through a comparison of HHG from bulk crystals and exfoliated flakes, we show the important role played by reabsorption of the generated harmonics in determining the overall efficiency and find that the generated harmonics are consistent with a strong high-order perturbative nonlinear response. First-principles calculations of the laser-driven polarization currents in CIPS suggest that the strong nonlinearity originates from electron–electron correlations, marking the first observation of a correlation-mediated enhancement of HHG to the best of our knowledge. Since CIPS and other MTPs combine the advantages of three-dimensional (3D) and 2D materials, such as strong optical absorption in bulk crystals and low-dimensional enhancement of electronic interactions and optical nonlinearity, our results signify the potential for new approaches to materials design for optoelectronics, with the goal of generating efficient high-order nonlinear responses from layered solid-state materials to realize lightwave-driven electronics.

RESULTS AND DISCUSSION

Synthesis of CIPS Single Crystal. CIPS single crystals were synthesized using the general procedures outlined in refs 15 and 16. Briefly, we utilized a self-flux growth technique where P_2S_5 was the flux. The precursor P_2S_5 (prepared at 300 °C in an evacuated fused silica ampule for 12 h from Alfa Aesar Puratronic elements, >99.999% purity) was combined with Cu (Alfa Aesar Puratronic, 99.999% purity, further reduced in H_2) and In (Alfa Aesar, 99.999% purity) in the ratio $Cu/In/P_2S_5$ 1:1:3 in 2 mL Al_2O_3 crucibles. The crucibles were arranged in a standard flux growth configuration, with the growth crucible

https://doi.org/10.1021/jacs.4c04515
J. Am. Chem. Soc. 2024, 146, 24288−24295

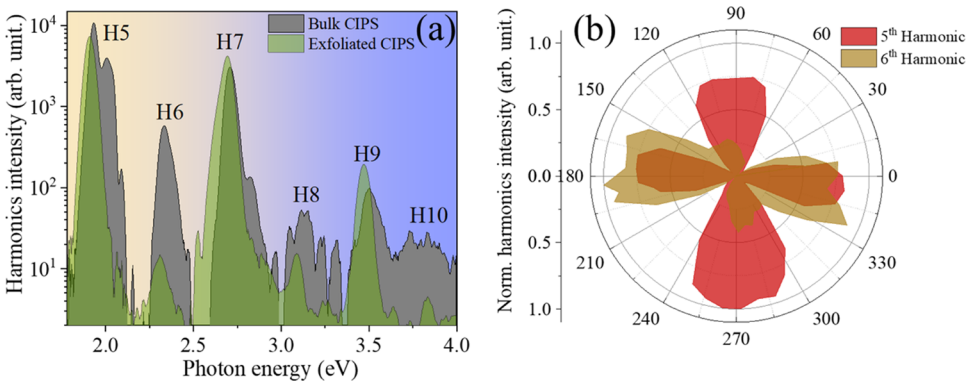

Figure 2. (a) HHG spectrum acquired from bulk and exfoliated CIPS with a driving laser wavelength of 3.2 μm at 1.6 and 0.9 TW/cm^2, respectively. (b) Polar plot depicting the polarization dependence of odd (fifth) and even (sixth) harmonics from a bulk CIPS.

on the bottom and an inverted crucible placed directly on top to catch any unreacted flux during centrifugation. We then sealed these crucibles in a fused silica ampule under ~250 Torr of Ar, heated them slowly to 650 °C, held them at that temperature for 36 h, and cooled them at a rate of 1.8 °C/h to 350 °C, where they were centrifuged to decant the flux. We then placed the ampule, upside-down, in the furnace at 350 °C and cooled it to room temperature at a rate of 10 °C/h. Sample compositions were determined by subjecting 3 distinct single-crystal specimens to multiple-spot scanning electron microscopy/energy-dispersive X-ray spectroscopy (SEM/EDS) analysis (i.e.,12 spots total) using a Thermo Scientific UltraDry EDS spectrometer joined with a JEOL JSM-6060 SEM. The EDS composition was found to be $CuInP_2S_6$, within experimental error. We also collected powder X-ray diffraction (XRD) data of the (00l) face of the crystal using a Bruker D8 DISCOVER DAVINCI system with Co Kα radiation (λ = 1.78897 Å) at room temperature. We used FullProf[17] to determine the layer spacing (defined as the sum of one lamella and one van der Waals gap) by setting the monoclinic angle to 90° and not refining the a or b lattice parameters.[18−20]

The as-grown CIPS crystal and mechanically exfoliated CIPS flakes (using the Scotch-tape method) are shown in Figure 1a,b, respectively. The bulk crystal used in the HHG experiments had a thickness of approximately 140 μm, as shown in Supporting Figure S1a. Our atomic force microscopy (AFM) analysis, shown in Figure 1c, indicates that the thickness of the exfoliated CIPS is approximately 180 nm, and the sample therefore contains hundreds of monolayers. The bulk CIPS crystal (Figure 1a) exhibits a nearly hexagonal growth pattern, as is common in MTP crystal growth. Additional characterization performed on the CIPS crystals used in experiments, including X-ray diffraction and photoluminescence (PL) measurements, indicate a high-purity crystal with monoclinic symmetry. These measurements are shown in Figure S1b,c and are consistent with prior characterization of CIPS crystals produced by the same group, indicating a phase-pure material.[20,21]

Higher Harmonic Generation from CIPS. For studies of high-order harmonic generation (HHG) in CIPS, we focused intense mid-infrared femtosecond laser pulses onto the sample and detected the harmonics in transmission geometry, as shown schematically in Figure 1d. Mid-infrared pulses were produced by a two-stage optical parametric amplifier (OPA, Light Conversion ORPHEUS-ONE), which was pumped by a Yb:KGW amplifier (KGW, potassium gadolinium tungstate; Light Conversion Carbide). The OPA idler is tunable from 2.2 to 4.5 μm, and ~10 μJ, 90 fs pulses at the central wavelength of 3.2 μm were selected for the present experiments. The linearly polarized OPA output beam was focused onto the sample using a 10 cm focal length lens, resulting in a beam waist (diameter) of approximately 60 μm and a peak intensity of up to 7 TW/cm^2. The harmonics emitted from the sample were collected in a transmission geometry and focused onto the entrance slit of a high-resolution UV/vis spectrometer (Ocean Optics HR2000+ES) to record the spectrum. For exfoliated samples, the crystals were supported on the entrance plane of a c-plane Al_2O_3 substrate with a 100 μm thickness. No harmonics were observed from the Al_2O_3 substrate alone at the intensities used in the experiments.

Figure 2a (Supporting Information, Figure S1d) shows the harmonic spectra acquired from the bulk and exfoliated CIPS crystals on a logarithmic intensity scale. We observe distinct harmonic peaks, corresponding to even and odd harmonics ranging from the 5th harmonic order (1.96 eV) to the 10th harmonic order (3.81 eV). In comparison to the exfoliated samples, the bulk crystal exhibits broader harmonic peaks that are shifted toward the high-frequency side of the spectrum, which can be attributed to nonlinear propagation and blue-shifting of the driving laser in the bulk medium.

The spectra from both samples consist of strong odd and weak even harmonic orders. Due to its noncentrosymmetric space group Cc at room temperature, the generation of even harmonics in CIPS is expected to occur for driving laser polarization along the crystal's c-axis.[22] To validate this, we performed polarization-dependent measurements of HHG on the bulk (Figure 2b) and exfoliated (Supporting Information, Figure S2) crystals, in which the harmonic spectrum was measured for different driving laser polarizations with respect to the crystal axes. It can be seen clearly that the fifth harmonic exhibits a 4-fold symmetry, whereas the sixth harmonic has two symmetric lobes at 0 and 180°, corresponding to laser polarization along the c-axis. There is a weak remnant signal from the sixth harmonic at 90°, which could be due to birefringence in the bulk medium, imperfect alignment of the sample surface normal with respect to the driving laser propagation direction, or cascaded low-order nonlinear processes.

Next, we recorded the intensity dependence for harmonics generated in both the bulk and exfoliated samples by varying the intensity of the driving laser, the expected scaling behavior with the best fit obtained is shown in Figure 3a. To investigate

https://doi.org/10.1021/jacs.4c04515
J. Am. Chem. Soc. 2024, 146, 24288−24295

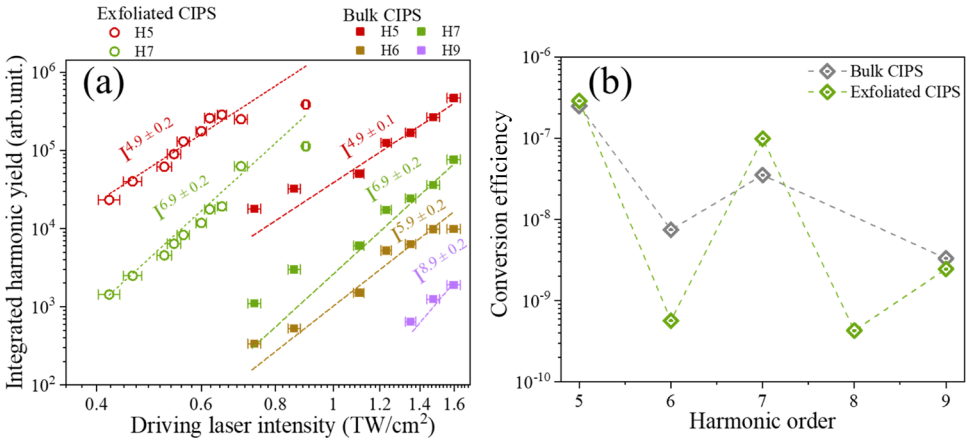

Figure 3. (a) Intensity dependence of the harmonic yield from bulk (filled squares) and exfoliated (empty circles) CIPS samples, along with power law scaling curves. The error bars are primarily determined by variation in the measurements of the driving laser pulse energy. (b) Measured conversion efficiencies of different harmonics obtained from bulk and exfoliated flakes of CIPS. Conversion efficiency as high as 10^{-7} is obtained for the fifth and seventh harmonics generated in the exfoliated sample, while even stronger harmonic generation is observed from the bulk sample.

Table 1. Comparison of the Conversion Efficiency of HHG with Different Materials

sample	conversion efficiency	type of process	mechanism of HHG	reference
ZnO crystal (thickness 300 μm)	10^{-6}–10^{-7} (11th to 17th harmonic)	HHG	nonperturbative	23
GaP metasurface (thickness 400 nm)	2×10^{-9} (7th harmonic)	HHG	perturbative	25
CdTe crystal (thickness 1 mm)	2.3×10^{-5} (5th to 8th harmonic)	HHG	nonperturbative	26
monolayer MoS_2 (thickness 0.65 nm)	10^{-11} (5th and 7th harmonic)	HHG	nonperturbative	27,28
periodically poled $LiNbO_3$ waveguide	10^{-6} (5th harmonic at low power)	HHG	perturbative	29
$CuInP_2S_6$ bulk (143 μm) and thin flakes (180 nm)	10^{-7} (5th harmonic)	HHG	perturbative	present work

the scaling, we have performed power law fits to the experimental data, excluding the last data point from the fits for all but the ninth harmonic of the bulk sample to avoid discrepancies due to the saturation of several harmonic orders at the highest driving intensity. These measurements reveal two interesting features. First, we find that, while both the bulk and exfoliated crystals generate harmonics with similar strengths, harmonics are generated from the exfoliated sample with lower driving laser intensity. Second, the harmonics from both samples scale follow a power law scaling with the driving laser intensity. It is well known that harmonics generated in the perturbative regime of nonlinear optics obey the intensity scaling law $I_q \propto I_0^q$, where I_0 and I_q are the intensities of the driving laser and harmonic fields, respectively, and q is the harmonic order. Harmonic generation via nonperturbative processes[23] or cascaded nonlinearity[24] can lead to deviations from the power law intensity scaling. Based on the good agreement with the perturbative scaling shown in Figure 3a, we infer that harmonics are generated from both the bulk and exfoliated crystals in the perturbative regime and that cascaded nonlinearities do not play a substantial role.

Some deviations of the experimental data from the perturbative scaling are observed. At the lowest driving laser intensities, the nonlinear signal strength is very weak, and therefore, it is subject to measurement noise. Both additive and shot noises can cause deviations from the expected power law behavior. Importantly, these data points introduce only a small uncertainty in the least-squares fitting, as the deviations of the experimental data from the fitting function are small on an absolute scale. At the highest intensities studied, saturation of the harmonics could indicate a transition from the perturbative to nonperturbative regime, or it could indicate that self-action effects on the driving pulse become important at these intensities. Finally, increasing the intensity beyond 1.6 TW/cm^2 for bulk CIPS results in the irreversible disappearance of the harmonic spectrum due to crystal damage. A quantitative understanding of these deviations of the experimental data from the perturbative response, and their physical origin, would benefit further understanding of the HHG response from layered materials but is beyond the scope of this paper.

Finally, we directly measured the conversion efficiency (for details of the measurement, see the Supporting Information, Section 3) of each harmonic using a calibrated Si photodiode that is unresponsive to the mid-IR driving laser. As shown in Figure 3b, we observed conversion efficiencies as high as 10^{-7} for the fifth and seventh harmonics in the exfoliated samples. For the bulk sample, the conversion efficiencies for the fifth and seventh harmonics are modestly lower, suggesting that strong reabsorption of HHG in the bulk medium restricts the observation of near- and above-gap harmonics to only those generated very close to the exit plane of the crystal, as is expected for above-bandgap harmonics. This is consistent with the photoluminescence (PL) measurement (shown in Supporting Information, Figure S1c), which suggests the presence of below-gap defect states that can absorb light in the vicinity of the fifth harmonic. We note that these defects mainly consist of stacking faults and the presence of vacant sites, which are common in van der Waals gapped materials.

The measured conversion efficiencies are consistent with our group's prior measurements of high-order harmonic generation in bulk materials,[23] but are significantly higher than what we have observed for harmonic generation from nonphase matched perturbative nonlinear processes.[25] A detailed comparison of the conversion efficiencies of HHG from different materials, along with the observed nonlinear scaling behavior, is given in Table 1. From the table, we infer that

https://doi.org/10.1021/jacs.4c04515
J. Am. Chem. Soc. 2024, 146, 24288−24295

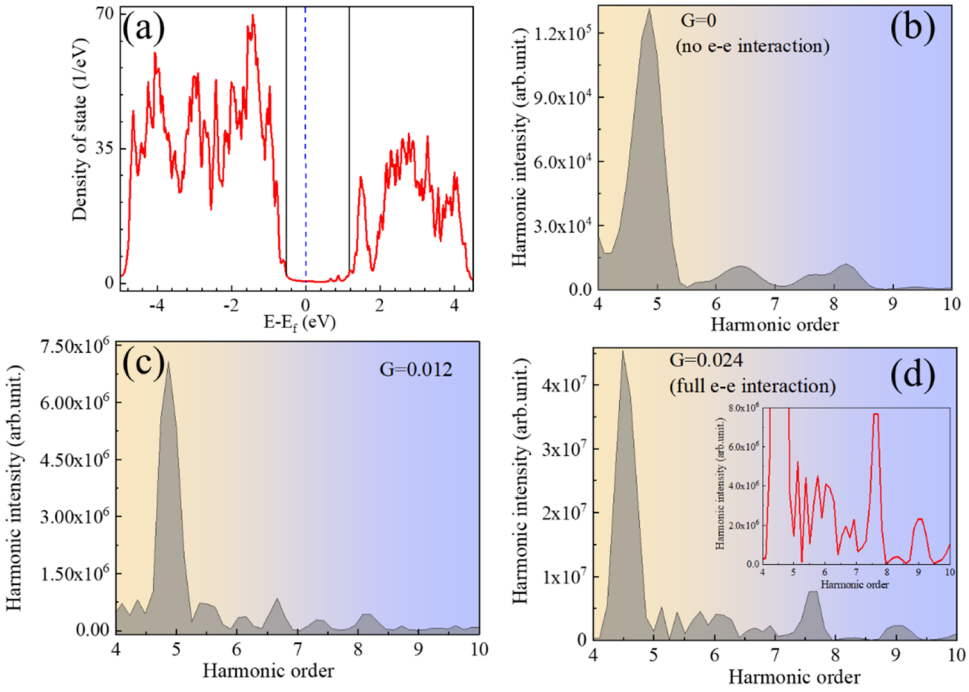

Figure 4. (a) Density of states (DOS) of CIPS obtained with DFT calculations. Orbital-resolved DOS are given in the Supporting Information. (b) The HHG spectrum of CIPS obtained with no electron−electron interaction. (c, d) The HHG spectrum of $CuInP_2S_2$ obtained at different strengths of the electron−electron interaction. In (d), the inset shows the suppression of HHG emission in the vicinity of the eighth harmonic and enhancement in the vicinity of the ninth harmonic.

HHG conversion efficiency of CIPS is comparable to nonperturbative HHG efficiencies reported in the literature but can be obtained at several times lower peak intensity and that the conversion efficiency is orders of magnitude higher than what has been observed in perturbative high-order harmonic generation. The latter observation is suggestive of extraordinary fifth- and seventh-order optical nonlinearity in CIPS.

Theoretical Analysis. We next investigated the origin of the extraordinary nonlinear response of CIPS through time-dependent density functional theory (TDDFT) calculations, which included the effects of electron correlations. First, the static properties of the system were calculated from DFT by using the plane-wave and pseudopotential methods as implemented in the Quantum Espresso package.[30] The exchange and correlation effects were taken into account with the local density approximation (LDA) in the form of Perdew−Zunger (PZ),[31] and we used projector augmented wave (PAW) pseudopotentials to describe the core−valence interactions. The side and top views of the used CIPS unit cell are shown in Supporting Figure S3.

We described the valence wave functions and the electron density by plane-wave basis sets with kinetic energy cutoffs of 70 and 280 Ry, respectively. We sampled the first Brillouin zone with a 5 × 5 × 5 Monkhorst−Pack grid and optimized atomic positions and lattice parameters, until the residual forces converged to less than 0.01 eV/Å. We would like to note that the used *k*-point mesh is ∼2 times larger in "*a*" direction, compared to the other two directions. To make the mesh almost homogeneous, one needs to use 100% more *k*-points, which would significantly slow down the calculations. Although the momentum steps in all directions are rather small, the used inhomogeneous mesh gives accurate results. In the TDDFT calculations, the DFT bandgap of 1.4 eV was shifted to the experimental value of 2.7 eV.[12] The TDDFT analysis was performed by using the DMFT XC kernel obtained from the solution of the effective Hubbard model.[32,33] It is important to emphasize that the Coulomb repulsion for the s- and p-states is an order of magnitude smaller than for d-states and usually plays a minor role. We used the DFT spectrum as an approximation for the "free-electron" system. The correlation effects were included only in the analysis of the dynamics of the system, i.e., the electrons experience Coulomb repulsion where they meet on d-orbitals of Cu atoms. Thus, it is assumed that an electron that arrives on the already occupied Cu(-d) site has energy larger by the value of the local Coulomb repulsion *U*. The main effect of *U* correction in the static calculations would be a shift of the value of the bandgap, and we already indirectly included this effect by shifting the gap to the experimental value. The DFT density of states is shown in Figure 4a. For further details of the approach, we refer the reader to ref 34.

TDDFT Calculations, Electron−Electron Interactions, and the HHG Spectrum. Since the correlated d-orbitals of the Cu atoms give a major contribution to the states at the top valence bands, correlation effects are expected to play an important role in the response of the system (see Supporting Information, Figures S4−S7), and the generation of odd seventh and ninth harmonics can be attributed to correlated Cu d-orbital holes. It follows from our calculations (Supporting Information, Figures S4 and S5) that the d-orbital DOS in the valence band for the In atoms is 2 orders of magnitude smaller than for the Cu atoms. Therefore, we did not take into account the correlation effects for the In d states. It must be noted that in addition to the band structure, the quasi-particle wave functions can also define the nonlinear response of materials. However, early studies (by Levine et al.) show that there is no significant difference between the LDA and gravitational wave

https://doi.org/10.1021/jacs.4c04515
J. Am. Chem. Soc. 2024, 146, 24288−24295

(GW) functions for bulk systems.[35] Similarly, the wave functions for bulk materials are often similar in the DFT and DFT+U cases. However, in the case of lower dimensions, like in the studied layered system, this problem requires a separate analysis. In the TDDFT calculations, we used six bands (one valence and five conduction bands which are closely spaced in energy), and the laser pulse was modeled by a truncated cosine function given as

$$\vec{E}(t) = \vec{E}_0 \cos^2\left(\frac{\pi(t-\tau_c)^2}{2\tau_p^2}\right)\cos(\omega_0(t-\tau_c))$$

$$\text{when } (t-\tau_c)^2 | t-\tau_c | \leq \tau_p$$

with the parameters ω_o = 0.38 eV, E_o = 0.1 eV/Å and pulse duration τ = 86 fs (64 fs fwhm). In calculations of the HHG spectrum with TDDFT, we have included effects of local-in-space (on-site) electron−electron interactions described by strength G, that has ab initio value 0.024 1/Å^3. The results for the HHG spectrum at different strengths of the electron−electron interactions are shown in Figure 4b−d. As follows from these figures, the dominating fifth harmonic is present in all cases, including the case of no interaction. Thus, it must be generated by nonlinear processes that do not rely on correlations. As the strength of the interaction increases, the system starts to generate well-pronounced peaks near sixth, seventh, and ninth harmonic energies, in good agreement with the experimental data. As in previous studies of HHG using TDDFT, the emission spectra do not show clear peaks at harmonic multiples of the driving laser frequency.[36] However, we have verified through simulations with different driving laser frequencies that the observed spectra do correspond to HHG (see Supporting Information, Figure S8a), and therefore comparisons between the experiments and simulations can still be made based on the spectral intensities in certain spectral regions. As the strength of the interaction increases, the spectral weight shifts toward higher frequencies, and spectral features emerge that agree qualitatively with the experimentally measured spectra. The shift of spectral weight toward higher harmonic orders, and the enhancement of odd orders relative to even can be directly related to electron−electron interactions, since the Coulomb interaction part in the density-matrix TDDFT equation is proportional to the product of three (odd number) polarization functions. More generally, prior studies of HHG within the Mott−Hubbard model[37] and dynamical mean-field theory[34] have also shown shifts in the spectral weight of the high-order harmonic spectrum toward higher frequencies with increased correlation strength. While previous experimental studies have demonstrated correlation-mediated enhancements in low-order optical nonlinearities,[38] to our knowledge, this is the first experimental observation of a similar enhancement in high-order nonlinearity.

CONCLUSIONS

In conclusion, we demonstrate, both experimentally and theoretically, the generation of higher harmonics in bulk and thin flakes of the layered copper indium thiophosphate crystal. When driving the material with femtosecond mid-infrared laser pulses, high-order nonlinear response and optical emission up to the 10th harmonic order was observed. The conversion efficiency of HHG from CIPS is similar to that from more commonly used crystals, and due to its layered van der Waals structure, CIPS appears promising as a platform for applications of strong-field nonlinear optics in the 2D limit. Furthermore, first-principles calculations of the microscopic currents responsible for HHG reveal that the observation of high-order harmonic orders may be linked to electron−electron interactions. These findings may aid in the exploration of novel nonlinear optical materials and nanophotonics platforms for efficient frequency conversion and lightwave electronics.

ASSOCIATED CONTENT

Supporting Information

The Supporting Information is available free of charge at https://pubs.acs.org/doi/10.1021/jacs.4c04515.

Additional experimental details, X-ray diffraction (XRD), photoluminescence (PL), cross-sectional optical image, polarization dependence of exfoliated CIPS, and TDDFT calculations (PDF)

AUTHOR INFORMATION

Corresponding Author

Michael Chini − *Department of Physics, University of Central Florida, Orlando, Florida 32816, United States;* Present Address: Department of Physics, The Ohio State University, Columbus, Ohio 43210, United States; Email: chini.4@osu.edu

Authors

Aamir Mushtaq − *Department of Physics, University of Central Florida, Orlando, Florida 32816, United States;* orcid.org/0000-0003-1845-8266

Troie Journigan − *Department of Physics, University of Central Florida, Orlando, Florida 32816, United States*

Volodymyr Turkowski − *Department of Physics, University of Central Florida, Orlando, Florida 32816, United States*

Ryan Siebenaller − *Department of Materials Science and Engineering, The Ohio State University, Columbus, Ohio 43210, United States; Materials and Manufacturing Directorate, Air Force Research Laboratory, Wright-Patterson Air Force Base, Ohio 45433, United States*

Dylan A. Jeff − *Department of Physics, University of Central Florida, Orlando, Florida 32816, United States; NanoScience Technology Center, University of Central Florida, Orlando, Florida 32826, United States*

Tran-Chau Truong − *Department of Physics, University of Central Florida, Orlando, Florida 32816, United States*

Mohamed Yaseen Noor − *Department of Materials Science and Engineering, The Ohio State University, Columbus, Ohio 43210, United States*

Dipendra Khatri − *Department of Physics, University of Central Florida, Orlando, Florida 32816, United States*

Christopher Lantigua − *Department of Physics, University of Central Florida, Orlando, Florida 32816, United States*

Kamal Harrison − *Department of Physics, University of Central Florida, Orlando, Florida 32816, United States; NanoScience Technology Center, University of Central Florida, Orlando, Florida 32826, United States*

Saiful I. Khondaker − *Department of Physics, University of Central Florida, Orlando, Florida 32816, United States; NanoScience Technology Center, University of Central Florida, Orlando, Florida 32826, United States*

Emmanuel Rowe − *Materials and Manufacturing Directorate, Air Force Research Laboratory, Wright-Patterson Air Force*

Base, Ohio 45433, United States; National Research Council, Washington, District of Columbia 20001, United States

Jonathan T. Goldstein − *Materials and Manufacturing Directorate, Air Force Research Laboratory, Wright-Patterson Air Force Base, Ohio 45433, United States*

Michael A. Susner − *Materials and Manufacturing Directorate, Air Force Research Laboratory, Wright-Patterson Air Force Base, Ohio 45433, United States;* orcid.org/0000-0002-1211-8749

Enam Chowdhury − *Department of Materials Science and Engineering, The Ohio State University, Columbus, Ohio 43210, United States*

Complete contact information is available at: https://pubs.acs.org/10.1021/jacs.4c04515

Notes

The authors declare no competing financial interest.

■ ACKNOWLEDGMENTS

This research was primarily supported by the Air Force Office of Scientific Research (AFOSR) under award no. FA9550-20-1-0284. Work performed at The Ohio State University was supported by the AFOSR Grant LRIR 23RXCOR003, AOARD-MOST Grant F4GGA21207H002, and AFOSR award no. FA9550-20-1-0278. The authors acknowledge support from the National Research Council's Senior NRC Associateship program sponsored by the National Academies of Sciences, Engineering, and Medicine. T. J., K.H., S.I.K., and M.C. acknowledge support from DMR 2121953 from NSF Partnerships for Research and Education in Materials (PREM). The authors also thank Prof. Roberto C. Myers from The Ohio State University for measurements of the room-temperature PL spectrum.

■ REFERENCES

(1) Ghimire, S.; Reis, D. A. High-harmonic generation from solids. *Nat. Phys.* **2019**, *15* (1), 10−16.

(2) Krausz, F.; Stockman, M. I. Attosecond metrology: from electron capture to future signal processing. *Nat. Photonics* **2014**, *8* (3), 205−213.

(3) Hui, D.; Alqattan, H.; Zhang, S.; Pervak, V.; Chowdhury, E.; Hassan, M. T. Ultrafast optical switching and data encoding on synthesized light fields. *Sci. Adv.* **2023**, *9* (8), No. eadf1015.

(4) Midorikawa, K. High-Order Harmonic Generation and Attosecond Science. *Jpn. J. Appl. Phys.* **2011**, *50* (9R), No. 090001.

(5) Ghimire, S.; DiChiara, A. D.; Sistrunk, E.; Agostini, P.; DiMauro, L. F.; Reis, D. A. Observation of high-order harmonic generation in a bulk crystal. *Nat. Phys.* **2011**, *7* (2), 138−141.

(6) Khan, A. R.; Zhang, L.; Ishfaq, K.; Ikram, A.; Yildrim, T.; Liu, B.; Rahman, S.; Lu, Y. Optical Harmonic Generation in 2D Materials. *Adv. Funct. Mater.* **2022**, *32* (3), No. 2105259.

(7) Jiang, T.; Huang, D.; Cheng, J.; Fan, X.; Zhang, Z.; Shan, Y.; Yi, Y.; Dai, Y.; Shi, L.; Liu, K.; Zeng, C.; Zi, J.; Sipe, J. E.; Shen, Y.-R.; Liu, W.-T.; Wu, S. Gate-tunable third-order nonlinear optical response of massless Dirac fermions in graphene. *Nat. Photonics* **2018**, *12* (7), 430−436.

(8) Elbanna, A.; Jiang, H.; Fu, Q.; Zhu, J.-F.; Liu, Y.; Zhao, M.; Liu, D.; Lai, S.; Chua, X. W.; Pan, J.; Shen, Z. X.; Wu, L.; Liu, Z.; Qiu, C.-W.; Teng, J. 2D Material Infrared Photonics and Plasmonics. *ACS Nano* **2023**, *17* (5), 4134−4179.

(9) Susner, M. A.; Chyasnavichyus, M.; McGuire, M. A.; Ganesh, P.; Maksymovych, P. Metal Thio- and Selenophosphates as Multifunctional van der Waals Layered Materials. *Adv. Mater.* **2017**, *29* (38), No. 1602852.

(10) Liu, F.; You, L.; Seyler, K. L.; Li, X.; Yu, P.; Lin, J.; Wang, X.; Zhou, J.; Wang, H.; He, H.; Pantelides, S. T.; Zhou, W.; Sharma, P.; Xu, X.; Ajayan, P. M.; Wang, J.; Liu, Z. Room-temperature ferroelectricity in $CuInP_2S_6$ ultrathin flakes. *Nat. Commun.* **2016**, *7* (1), No. 12357.

(11) Mushtaq, A.; Clink, L.; Noor, M. Y.; Kuz, C.; DeAngelis, E.; Siebenaller, R.; Fisher, A.; Verma, D.; Myers, R. C.; Conner, B. S.; Susner, M. A.; Chowdhury, E. Ultrafast Nonlinear Absorption and Second Harmonic Generation in $Cu_{0.33}In_{1.30}P_2S_6$ van der Waals Layered Crystals. *J. Phys. Chem. Lett.* **2022**, *13* (45), 10513−10521.

(12) Yan, X.-Q.; Zhao, X.; Xu, H.; Zhang, L.; Liu, D.; Zhang, Y.; Huo, C.; Liu, F.; Xie, J.; Dong, X.; Liu, Z.-B.; Tian, J.-G. Temperature-tunable optical properties and carrier relaxation of $CuInP_2S_6$ crystals under ferroelectric-paraelectric phase transition. *J. Mater. Chem. C* **2022**, *10* (2), 696−706.

(13) Rahman, S.; Yildirim, T.; Tebyetekerwa, M.; Khan, A. R.; Lu, Y. Extraordinary Nonlinear Optical Interaction from Strained Nanostructures in van der Waals $CuInP_2S_6$. *ACS Nano* **2022**, *16* (9), 13959−13968.

(14) Wang, X.; Du, K.; Liu, W.; Hu, P.; Lu, X.; Xu, W.; Kloc, C.; Xiong, Q. Second-harmonic generation in quaternary atomically thin layered $AgInP_2S_6$ crystals. *Appl. Phys. Lett.* **2016**, *109* (12), No. 123103.

(15) Rao, R.; Selhorst, R.; Jiang, J.; Conner, B. S.; Siebenaller, R.; Rowe, E.; Giordano, A. N.; Pachter, R.; Susner, M. A. Investigating Strain between Phase-Segregated Domains in Cu-Deficient $CuInP_2S_6$. *Chem. Mater.* **2023**, *35* (19), 8020−8029.

(16) Chica, D. G.; Iyer, A. K.; Cheng, M.; Ryan, K. M.; Krantz, P.; Laing, C.; dos Reis, R.; Chandrasekhar, V.; Dravid, V. P.; Kanatzidis, M. G. P_2S_5 Reactive Flux Method for the Rapid Synthesis of Mono- and Bimetallic 2D Thiophosphates $M_{2-x}M'_xP_2S_6$. *Inorg. Chem.* **2021**, *60* (6), 3502−3513.

(17) Frontera, C.; Rodríguez-Carvajal, J. FullProf as a new tool for flipping ratio analysis: further improvements. *Phys. B* **2004**, *350* (Suppl 1), E731−E733.

(18) McGuire, M. A.; Dixit, H.; Cooper, V. R.; Sales, B. C. Coupling of Crystal Structure and Magnetism in the Layered, Ferromagnetic Insulator CrI_3. *Chem. Mater.* **2015**, *27* (2), 612−620.

(19) Susner, M. A.; Rao, R.; Pelton, A. T.; McLeod, M. V.; Maruyama, B. Temperature-dependent Raman scattering and x-ray diffraction study of phase transitions in layered multiferroic $CuCrP_2S_6$. *Phys. Rev. Mater.* **2020**, *4* (10), No. 104003.

(20) Susner, M. A.; Belianinov, A.; Borisevich, A.; He, Q.; Chyasnavichyus, M.; Demir, H.; Sholl, D. S.; Ganesh, P.; Abernathy, D. L.; McGuire, M. A.; Maksymovych, P. High-Tc Layered Ferrielectric Crystals by Coherent Spinodal Decomposition. *ACS Nano* **2015**, *9* (12), 12365−12373.

(21) Susner, M. A.; Chyasnavichyus, M.; Puretzky, A. A.; He, Q.; Conner, B. S.; Ren, Y.; Cullen, D. A.; Ganesh, P.; Shin, D.; Demir, H.; McMurray, J. W.; Borisevich, A. Y.; Maksymovych, P.; McGuire, M. A. Cation−Eutectic Transition via Sublattice Melting in $CuInP_2S_6$/$In_{4/3}P_2S_6$ van der Waals Layered Crystals. *ACS Nano* **2017**, *11* (7), 7060−7073.

(22) Misuryaev, T. V.; Murzina, T. V.; Aktsipetrov, O. A.; Sherstyuk, N. E.; Cajipe, V. B.; Bourdon, X. Second harmonic generation in the lamellar ferrielectric $CuInP_2S_6$. *Solid State Commun.* **2000**, *115* (11), 605−608.

(23) Gholam-Mirzaei, S.; Beetar, J.; Chini, M. High harmonic generation in ZnO with a high-power mid-IR OPA. *Appl. Phys. Lett.* **2017**, *110* (6), No. 061101.

(24) Park, H.; Camper, A.; Kafka, K.; Ma, B.; Lai, Y. H.; Blaga, C.; Agostini, P.; DiMauro, L. F.; Chowdhury, E. High-order harmonic generations in intense MIR fields by cascade three-wave mixing in a fractal-poled $LiNbO_3$ photonic crystal. *Opt. Lett.* **2017**, *42* (19), 4020−4023.

(25) Shcherbakov, M. R.; Zhang, H.; Tripepi, M.; Sartorello, G.; Talisa, N.; AlShafey, A.; Fan, Z.; Twardowski, J.; Krivitsky, L. A.; Kuznetsov, A. I.; Chowdhury, E.; Shvets, G. Generation of even and odd high harmonics in resonant metasurfaces using single and

multiple ultra-intense laser pulses. *Nat. Commun.* **2021**, *12* (1), No. 4185.
(26) Long, Z.; Yang, H.; Tian, K.; He, L.; Qin, R.; Chen, Z.-Y.; Wang, Q. J.; Liang, H. High-harmonic generation in CdTe with ultra-low pump intensity and high photon flux. *Commun. Phys.* **2023**, *6* (1), No. 228.
(27) Nishidome, H.; Nagai, K.; Uchida, K.; Ichinose, Y.; Yomogida, Y.; Miyata, Y.; Tanaka, K.; Yanagi, K. Control of High-Harmonic Generation by Tuning the Electronic Structure and Carrier Injection. *Nano Lett.* **2020**, *20* (8), 6215−6221.
(28) Liu, H.; Li, Y.; You, Y. S.; Ghimire, S.; Heinz, T. F.; Reis, D. A. High-harmonic generation from an atomically thin semiconductor. *Nat. Phys.* **2017**, *13* (3), 262−265.
(29) Hickstein, D. D.; Carlson, D. R.; Kowligy, A.; Kirchner, M.; Domingue, S. R.; Nader, N.; Timmers, H.; Lind, A.; Ycas, G. G.; Murnane, M. M.; Kapteyn, H. C.; Papp, S. B.; Diddams, S. A. High-harmonic generation in periodically poled waveguides. *Optica* **2017**, *4* (12), 1538−1544.
(30) Giannozzi, P.; Baroni, S.; Bonini, N.; Calandra, M.; Car, R.; Cavazzoni, C.; Ceresoli, D.; Chiarotti, G. L.; Cococcioni, M.; Dabo, I.; Dal Corso, A.; de Gironcoli, S.; Fabris, S.; Fratesi, G.; Gebauer, R.; Gerstmann, U.; Gougoussis, C.; Kokalj, A.; Lazzeri, M.; Martin-Samos, L.; Marzari, N.; Mauri, F.; Mazzarello, R.; Paolini, S.; Pasquarello, A.; Paulatto, L.; Sbraccia, C.; Scandolo, S.; Sclauzero, G.; Seitsonen, A. P.; Smogunov, A.; Umari, P.; Wentzcovitch, R. M. QUANTUM ESPRESSO: a modular and open-source software project for quantum simulations of materials. *J. Phys.: Condens. Matter* **2009**, *21* (39), No. 395502.
(31) Perdew, J. P.; Zunger, A. Self-interaction correction to density-functional approximations for many-electron systems. *Phys. Rev. B* **1981**, *23* (10), 5048−5079.
(32) Turkowski, V.; Rahman, T. S. Nonadiabatic exchange-correlation kernel for strongly correlated materials. *J. Phys.: Condens. Matter* **2017**, *29* (45), No. 455601.
(33) Acharya, S. R.; Turkowski, V.; Zhang, G. P.; Rahman, T. S. Ultrafast Electron Correlations and Memory Effects at Work: Femtosecond Demagnetization in Ni. *Phys. Rev. Lett.* **2020**, *125* (1), No. 017202.
(34) Alam, D.; Ud Din, N.; Chini, M.; Turkowski, V. Electron-electron interactions and high-order harmonics in solids. *Phys. Rev. B* **2022**, *106* (23), No. 235124.
(35) Levine, Z. H.; Allan, D. C. Linear optical response in silicon and germanium including self-energy effects. *Phys. Rev. Lett.* **1989**, *63* (16), 1719−1722.
(36) Floss, I.; Lemell, C.; Wachter, G.; Smejkal, V.; Sato, S. A.; Tong, X.-M.; Yabana, K.; Burgdörfer, J. Ab initio multiscale simulation of high-order harmonic generation in solids. *Phys. Rev. A* **2018**, *97* (1), No. 011401.
(37) Silva, R. E. F.; Blinov, I. V.; Rubtsov, A. N.; Smirnova, O.; Ivanov, M. High-harmonic spectroscopy of ultrafast many-body dynamics in strongly correlated systems. *Nat. Photonics* **2018**, *12* (5), 266−270.
(38) Wang, K.; Seidel, M.; Nagarajan, K.; Chervy, T.; Genet, C.; Ebbesen, T. Large optical nonlinearity enhancement under electronic strong coupling. *Nat. Commun.* **2021**, *12* (1), No. 1486.

https://doi.org/10.1021/jacs.4c04515
J. Am. Chem. Soc. 2024, 146, 24288−24295